

First microlensing candidate towards M31 from Nainital Microlensing Survey

Y. C. Joshi^{1,2}, A. K. Pandey², D. Narasimha^{1,3}, R. Sagar²

¹ Tata Institute of Fundamental Research, Homi Bhabha Road, Mumbai – 400 005, India

² Aryabhatta Research Institute of Observational Sciences (ARIES), Manora peak Nainital - 263129, India

³ Astronomical Institute, Tohoku University, Sendai 980-8578

Received 12 November 2004 / Accepted 20 December 2004

Abstract. We report our first microlensing candidate NMS-E1 towards M31 from the data accumulated during four years long Nainital Microlensing Survey. Cousin R and I band observations of $\sim 13' \times 13'$ field in the direction of M31 were carried out since 1998 and data is analysed using pixel technique proposed by the AGAPE collaboration. The NMS-E1 lies in the disk of M31 at $\alpha = 0^h 43^m 33\rlap{.}^s.3$ and $\delta = +41^\circ 06' 44''$, about 15.5 arcmin away in the South-East direction from the center of M31. The degenerate Paczyński fit gives a half intensity duration of ~ 59 days. The photometric analysis of candidate shows that it reached up to $R \sim 20.1$ mag at the time of maximum brightness and colour of the source star estimated to be $(R - I)_0 \sim 1.1$ mag. It is seen that the microlensing candidate is blended by red variable stars consequently light curves do not strictly follow the characteristic Paczyński shape and achromatic nature however its long period monitoring and similar behaviour in R and I bands lend support of its microlensing nature.

Key words. dark matter — galaxies:halos — galaxies:individual (M31) — observations — cosmology: gravitational lensing

1. Introduction

Recent years have seen rapid advances in our understanding of the nature of dark matter in the Galaxy. Much of this progress has come from gravitational microlensing, a phenomenon of temporary amplification of the flux of a background star when a foreground MACHO passes close to our line of sight to this background star. In the last decade, several collaborations have focussed their attention towards Galactic bulge and Magellanic Clouds following the suggestion of Paczyński (1986) and reported more than one thousand microlensing events after monitoring millions of star in these directions (e.g. Alcock et al. 1993 for MACHO, Udalski et al. 1993 for OGLE and Aubourg et al. 1993 for EROS collaborations). These groups have ruled out most of the dark matter in the form of sub-stellar objects and estimated that only up to 20% of the halo could be formed of MACHOs in the mass range of $0.15 M_\odot$ to $0.9 M_\odot$ (Alcock et al. 2000., Lasserre et al. 2000).

Though the conventional microlens monitoring is a great success towards Galactic bulge and Magellanic Clouds, it is fundamentally limited to only nearby regions where there are large number of resolved stars. In the far-off regions like M31, which is at a distance of \sim

780 kpc (Stanek & Garnovich 1998, Joshi et al. 2003), microlens monitoring is a cumbersome process due to the large background of unresolved stars of M31 where typical stellar density is as high as few hundred stars per arcsec². To deal with the problem, Baillon et al. (1993) proposed to monitor pixels of the CCD rather than the stars themselves. Any variation in the flux of stars due to microlensing would reflect to the corresponding variation in the pixel of the CCD. Therefore, by monitoring a pixel for a long duration of time, one can actually detect a microlensing event. The pixel technique which relies on the shape analysis of the light curve to detect microlensing events is implemented by the AGAPE (Ansari et al. 1997) and POINT-AGAPE collaborations (Paulin-Henriksson et al. 2002); and reported more than 10 possible microlensing events towards M31 (Calchi Novati et al. 2002, 2003, Paulin-Henriksson et al. 2002, 2003). A similar approach but based on the image subtraction technique was proposed by Crotts (1992) and Tomaney & Crotts (1996) that has been further improved by Alard & Lupton (1998) and Alard (2000) by optimal image subtraction using a space-varying kernel; and the technique is widely used to detect different kind of variable sources (cf. Bonanos et al. 2003; Taylor 2004). Recently MEGA collaboration has reported 14 microlensing candidates in their survey to-

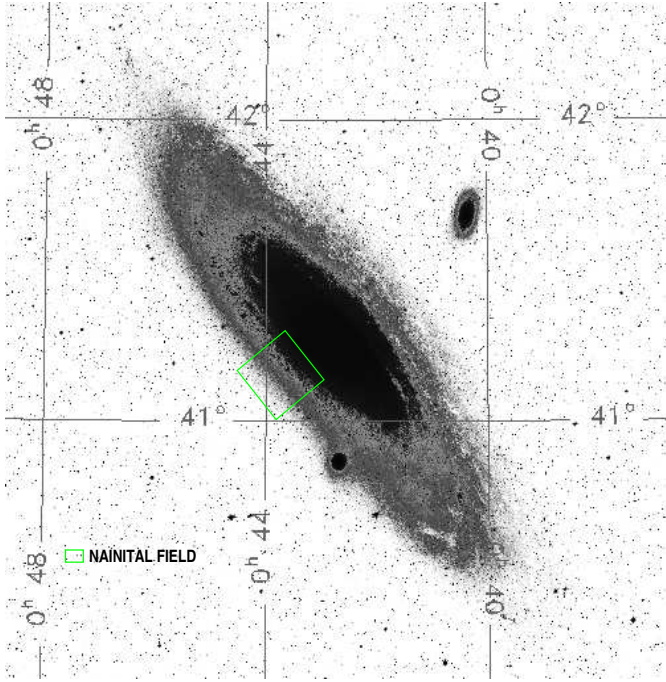


Fig. 1. A $13' \times 13'$ field of Nainital Microlensing Survey juxtaposed over M31.

wards M31 using the image subtraction technique (de Jong et al. 2003). Two of them (ML-7 and ML-11) have already been reported by POINT-AGAPE in their survey using pixel technique (PA-99-N2 and PA-00-S4 respectively). It is worth mentioning that both the groups give similar results though derived through two different techniques.

Though pixel lensing technique allows us to detect microlensing events where standard technique of microlens detection is not applicable, it is limited to only bright stars which are either giants and super-giants or stars that are amplified enough to become detectable above the noise level of background flux. Since the search for gravitational microlensing events requires monitoring of millions of stars over a few years to yield a significant number of microlens detection as well as to test their uniqueness characteristics, we started multi-band observations of M31 in the autumn of 1998 under a program **Nainital Microlensing Survey** at the ARIES, Nainital, India in the collaboration with the AGAPE (Joshi 2004). The details of our observations are given in the next section while the pixel technique and its implementation in our data is described in Sect. 3. The selection criteria of microlensing search and our results are given in Sect. 4 followed by the discussion and conclusions.

2. Observations

We started Cousins R and I band observations in the direction of M31 in 1998, with a small $1K \times 1K$ CCD covering an area of $\sim 6' \times 6'$ at the $f/13$ Cassegrain focus of 104-cm Sampurnanand Telescope. Since 1999, observa-

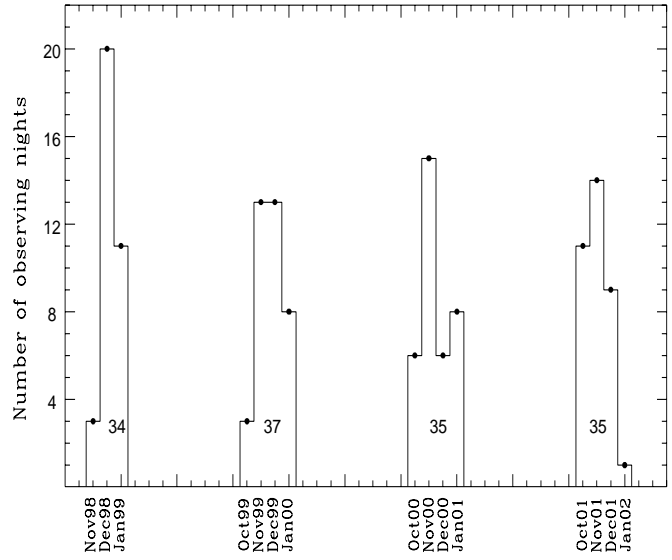


Fig. 2. A histogram of the data taken in 4 year long survey. The total number of nights observed per observing season is given in the box.

tions have been carried out with a larger size $2K \times 2K$ CCD chip which covers $\sim 13' \times 13'$ encompassing the previous field. Each pixel covers an area of 0.37×0.37 arcsec 2 of the sky. The target field is centered at $\alpha_{2000} = 0^h 43^m 38^s$ and $\delta_{2000} = +41^\circ 09'.1$, at a distance of about 15 arcmin away in the South-East direction from the center of M31. Fig. 1 shows the location of the target field superposed over the image of M31. In the 4 years observing run, we accumulated a total of 468 data points in R band and 383 data points in I band during 141 observational nights spanning over 1200 days. A histogram of the data taken in the survey is shown in Fig. 2. The average seeing during the observations was ~ 2.2 arcsec. A detailed overview of the observations is given in Joshi et al. (2003).

3. Pixel Method

The basic principle of the pixel method is that if a star of flux F_* is lensed in a crowded field, then by subtracting the original flux from the amplified flux of the star, one gets an increase in flux equal to $(A - 1)F_*$ above the photon noise where A is the magnification of star. Now if the target star shows a variation in the flux with time, it shall reflect in the ΔF of the pixel. Thus by following ΔF with time, we can actually monitor the variation in the flux of the target star. Although to detect any variation in the flux, this change should be significantly above the fluctuation level.

In the point-like lens and uniform motion approximation, magnification factor A is related to the impact parameter u as given by the following Eq.

$$A(t) = \frac{u^2(t) + 2}{u(t)\sqrt{u^2(t) + 4}} \quad (1)$$

where $u^2(t) = u_0^2 + \frac{(t-t_0)^2}{t_E^2}$. Here t_0 and t_E are the time of maximum amplification and Einstein time scale respectively and u_0 indicates the distance of closest approach in the units of Einstein radius. When $u(t) \ll 1$, the magnification is well approximated by

$$A(t) \equiv \frac{1}{u(t)}; \quad A_{max} \approx \frac{1}{u_0}$$

Then the change in flux of the target star is given by

$$\Delta F = \frac{F_* A_{max}}{\sqrt{1 + \left(\frac{t-t_0}{t_E/A_{max}}\right)^2}} \quad (2)$$

From the light curve of a resolved star, one can get three parameters namely peak time (t_0), Einstein time (t_E) and peak magnification (A_{max}) by fitting a theoretical light curve. However, for the unresolved stars as in the case of pixel lensing, there is a degeneracy among the t_E , A_{max} and F_* (Gould 1996). Hence, high quality data (e.g. Paulin-Henriksson et al. 2003) or detection of source star (e.g. Auriére et al. 2001) are required to accurately determine the t_E hence mass of the MACHO.

3.1. Implementation of pixel method in Nainital data

Standard CCD reduction technique was used for the pre-processing of data using IRAF¹ which includes bias subtraction, flat fielding and cosmic rays removal. We added all the frames of a particular filter taken on a single night and made one frame per filter per night to increase the signal to noise ratio.

3.1.1. Alignments

To align the images, we have to first select a reference frame which should be taken in a good photometric condition, lesser sky background and relatively small seeing. We choose an image taken on January 05, 2000 as a reference frame. The average seeing during the night was 1.5 arcsec.

Since the observations were carried out in different nights, a star does not fall onto the same pixel in all the images. Therefore, we align all the images through rotation and shifting with respect to the reference frame. We achieve an accuracy better than 0.05 arcsec in alignment for most of the images.

The photometric conditions like earth's atmospheric absorption and sky background are never the same for different nights. To bring all the images at same photometric level, we correct the images with respect to the reference frame using the statistical approach explained by Ansari et al. (1997). To overcome the residual gradient between two different frames due to reflected light, we normalize all the images with respect to the median background of reference frame.

¹ Image Reduction and Analysis Facility (IRAF) is distributed by the National Optical Astronomy Observations

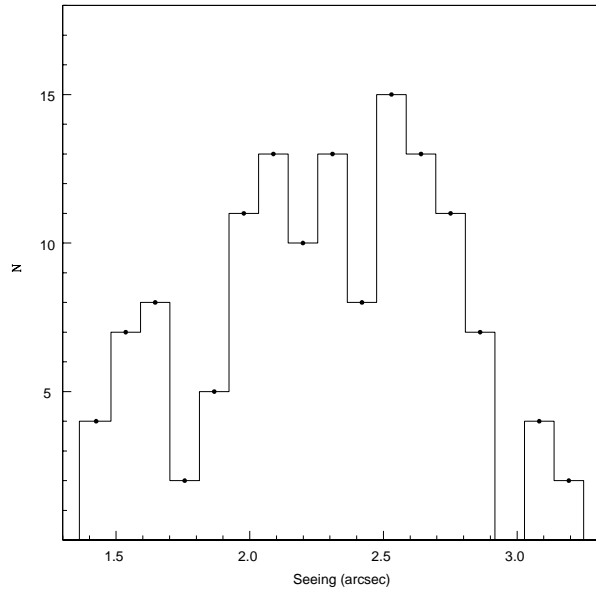


Fig. 3. A histogram of seeing distribution during four years observing period.

3.1.2. Seeing Correction

Most of our observations were carried out in the early hours of the night when sky condition might not have been perfectly stable resulting in large seeing which is conspicuous in Fig. 3 where we have plotted the histogram of seeing variation with the time in a four years long observing run. The seeing during our observations varies in a range of $\sim 1''.4$ to $3''.2$ with an average seeing of $2''.2$. The large seeing fluctuations during different observing periods may cause fake variation in the pixel light curve. To correct it, we make a superpixel of 7×7 pixel² ($\sim 2.5 \times 2.5$ arcsec² area of sky) around each pixel so that most of the stellar flux falls on that superpixel² though it only solves part of the seeing problem and does not correct for the loss of photon counts in the changing wings of PSF due to highly variable seeing between the frames. We thus correct the images by using AGAPE 'seeing stabilization method' (Calchi Novati et al. 2002, Paulin-Henriksson et al. 2002) where we assume on the basis of empirical observations that the difference in flux between any image and its median background is linearly correlated to the same difference for the reference image i.e.

$$\phi_i - \tilde{\phi}_i = \alpha_i(\phi_{ref} - \tilde{\phi}_{ref}) + \beta_i \quad (3)$$

where ϕ_{ref} and ϕ_i are the flux of reference and i^{th} images respectively while $\tilde{\phi}_{ref}$ and $\tilde{\phi}_i$ are the flux of their respective median background images. The α_i and β_i are the seeing correction coefficients for the i^{th} image. In Fig. 4, we have shown the linear correlation between $(\phi_{ref} - \phi_{ref})$ and $(\phi_{curr} - \tilde{\phi}_{ref})$ for two images, one is taken in good seeing and other one in bad seeing conditions. The α_i and β_i

² In the subsequent sections, we shall use the term 'pixel' instead of 'superpixel'

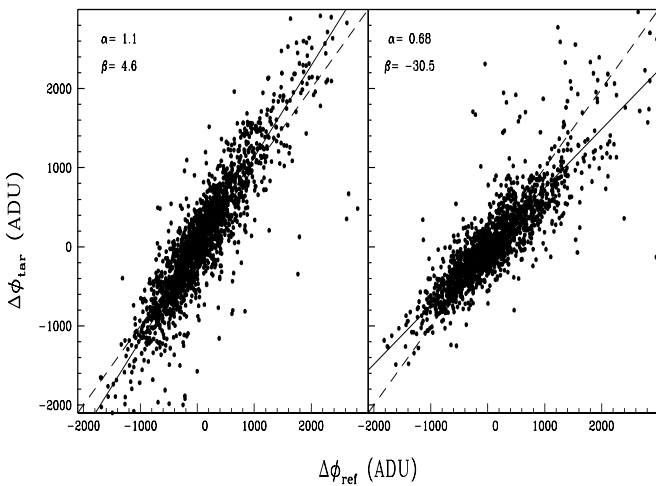


Fig. 4. Plot showing a linear correlation between the quantities $\Delta\phi_{tar} \equiv (\phi_{tar} - \tilde{\phi}_{tar})$ and $\Delta\phi_{ref} \equiv (\phi_{ref} - \tilde{\phi}_{ref})$. The left and right graphs show correlation for the images of good ($1''.4$) and bad ($2''.9$) seeing. The seeing of reference image is $1''.5$. The dashed lines are $y = x$ line while continuous lines indicate $y = \alpha x + \beta$ line.

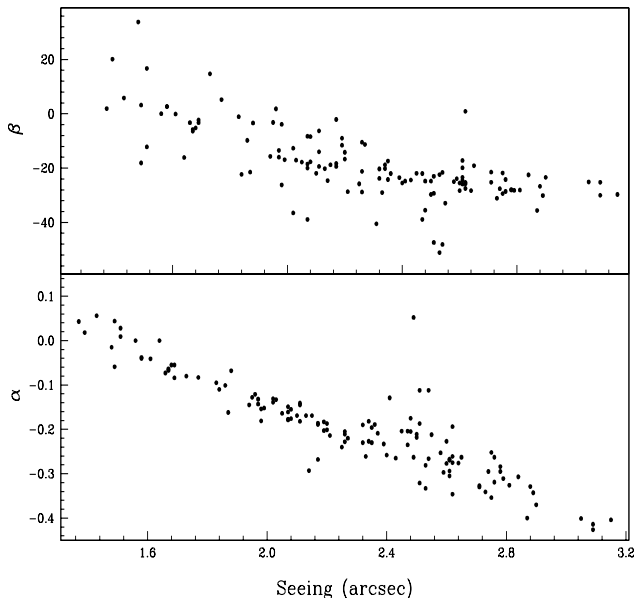


Fig. 5. The variation of seeing correction coefficients α and β as a function of seeing.

which are calculated with a χ^2 minimization procedure, shows a correlation with the seeing as shown in Fig. 5. After determining α and β for each image, we correct them by

$$\phi_i^{new} = \frac{\phi_i - \tilde{\phi}_i - \beta_i}{\alpha_i} + \tilde{\phi}_{ref} \quad (4)$$

where ϕ_i^{new} is the modified flux after seeing correction. This correction scales down all the images to the seeing of reference image.

3.2. Pixel light curves

To derive pixel light curve, we mask bad pixels which are either bright stars of which photometric analysis have already been carried out or contaminated due to spill-over of the saturated stars. In this way, we reject about 20% of the total pixels from the pixel analysis.

3.2.1. Stability of light curves

Since all the images are geometrically and photometrically aligned as well as seeing corrected, we expect the pixel light curve of non-variable objects to be stable with time. In Fig. 6, we illustrate the light curves of a stable pixel (782,579) in both R and I bands during its three year monitoring. The R.M.S. fluctuations along the light curve are ~ 97 and ~ 108 ADUs in R and I bands respectively which are less than the average error bars of ~ 166 and ~ 292 ADUs in the respective bands. This demonstrates that we have achieved a high level of stability in the pixel light curves after applying all the corrections.

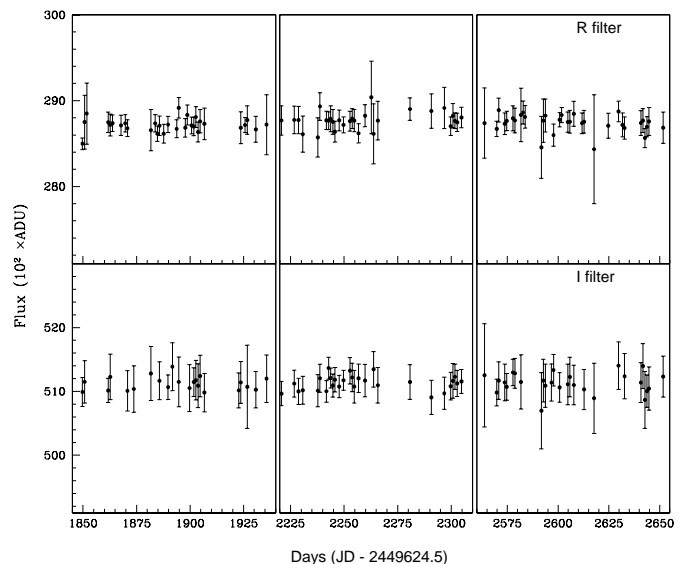


Fig. 6. The light curves of a non-varying pixel (782,579) in R and I bands during 1999-2001 observing season.

3.2.2. Comparison: Pixel vs Photometric light curves

To check the robustness of pixel technique in our data, we compare the pixel light curve of a star with its complementary light curve derived through photometric technique. However, for the comparison, we neither can take a very bright star where seeing correction used in pixel technique does not work well nor a very faint star where photometric error in magnitude determination is too large. Therefore, we choose a Cepheid of $R = 20.5$ mag having pixel coordinate (1186,595) for the comparison. From the data derived through pixel technique, we obtain a period of 7.457 ± 0.002 days for the Cepheid using period-searching

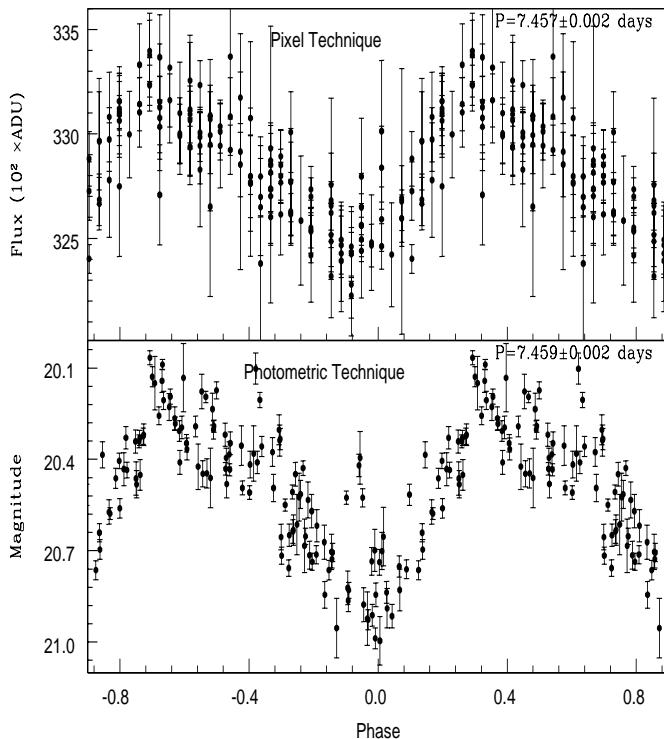


Fig. 7. The R band phase light curve of Cepheid (1186,595) derived through pixel and photometric techniques respectively. Phase is plotted twice and in such a way that the minimum brightness falls at zero phase. The flux and the magnitude derived through pixel and photometric techniques respectively are not scaled.

program given by Press & Rybici (1989). This value is in agreement with the period of 7.459 ± 0.002 days determined by Joshi et al. (2003). This supports the robustness of the pixel technique implemented in our data. For a comparison, the phase light curves obtained by these two different techniques are shown in Fig. 7. Nevertheless, we would like to mention that the photometric technique is better used for the resolved/bright stars while pixel technique is ideally suited in the case of unresolved/faint stars.

4. Search for microlensing events

The pixel method relies on the monitoring of flux variation of a pixel with time. To identify candidate pixels for the microlensing event, we adopt the same procedure as defined by Calchi Novati et al. (2002). Since R band data have better sampling density and photometric quality than that of the I band data, we used only R band data to select the light curves that are compatible with the microlensing event and I band data shall be latter used to analyse the microlensing candidate pixels. In the following sub-sections we briefly summarize the adopted procedure.

4.1. Selection Criteria

Initially we define a baselevel which is the minimum value of the sliding average flux of 9 consecutive points on the light curve. We thereafter define a bump in the light curve as 3 consecutive points rise above 3 sigma level and 2 consecutive points fall below 3 sigma level. Since there is about nine months gap between two consecutive observing seasons, we constrain all these points to be in the same observing run. For each bump, we define a likelihood function as

$$L = -\ln \left(\prod_{i \in \text{bump}} P(\phi > \phi_i | < \phi >_{i, \sigma_i}) \right) \quad (5)$$

where

$$P(\phi | \phi > \phi_i) = \int_{\phi_i}^{\infty} \frac{1}{\sigma_i \sqrt{2\pi}} \exp \left[-\frac{(\phi - \phi_{bkg})^2}{2\sigma_i^2} \right] d\phi$$

We chose only those pixels which have a primary bump with $L > 300$ and no secondary bump with $L > 70$ in the light curve. To exclude all those light curves which have more than one significant variations, we limit the ratio $\frac{L_{\text{secondary}}}{L_{\text{primary}}}$ not be greater than 0.1. We find ~ 19000 pixels which satisfy the above selection criteria. Most of them are cluster of pixels associated with significant physical variation. We clusterize these pixels and select only those pixels which have the highest value of L in their immediate neighbouring pixels. In this way we find 912 pixels characterized by the mono bump. To further check the flatness in the baseline of these pixels, we determine χ^2/N taking only those points which are used to determine baseline. A histogram of the χ^2/N for these pixels are shown in Fig. 8. To select the bumps with a flat baseline, we

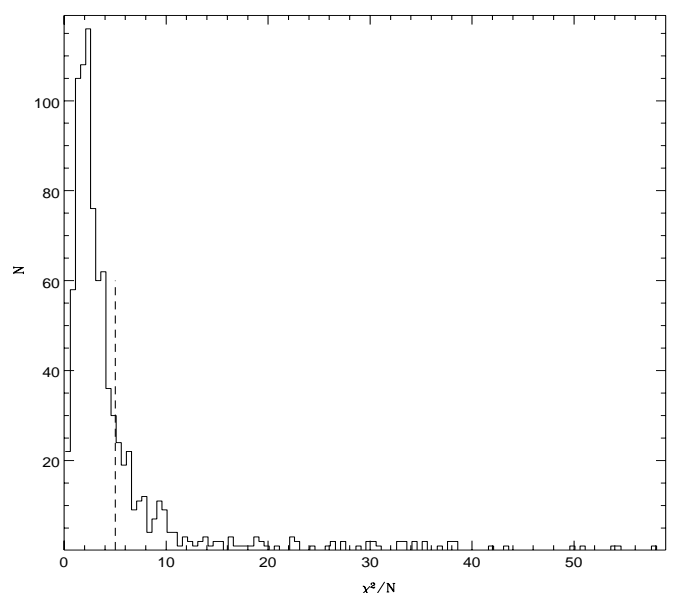


Fig. 8. A histogram of the χ^2/N for baseline flux. A vertical dashed line is drawn at $\chi^2/N = 5$, above which all the pixels were rejected.

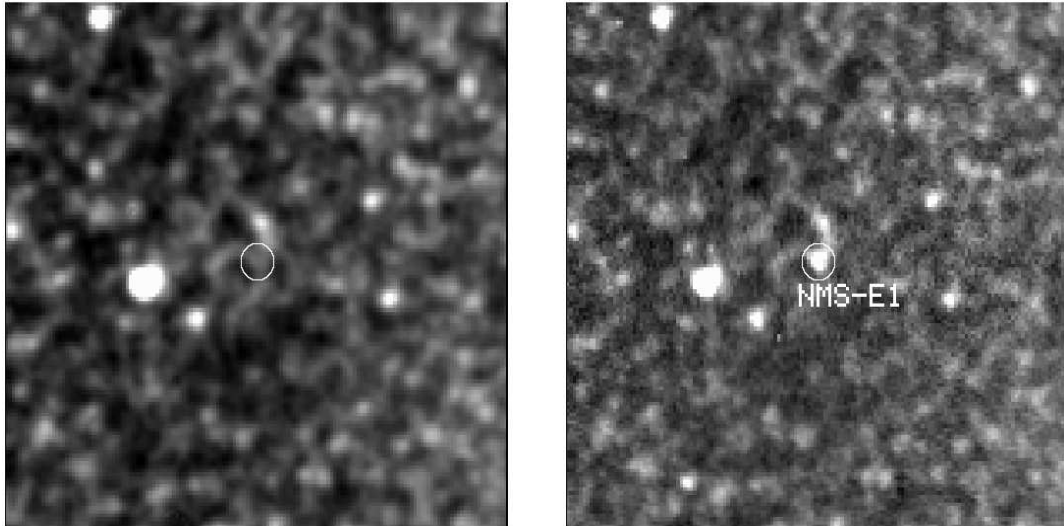


Fig. 9. The positions of NMS-E1 shown by the circle. The images are taken in I band. The left frame shows no brightness at the pixel (880,1402) while right frame shows a resolved star at that position.

reject all those pixels which have $\chi^2/N > 5$. This selection reduce the pixels to only 670 which are used for the shape analysis test. We do not put any selection criteria on $t_{1/2}$ as performed in some other surveys (e.g. Paulin-Henriksson et al. 2003, Riffeser et al. 2003) because of: *a*) observational gaps in our data which are as much as about 10 days between two consecutive nights within a single observing season; *b*) duration of the observations per season with an average observing density of once in three days; *c*) total period of our monitoring (> 800 days) is large enough to exclude any other kind of variability; and *d*) we are observing towards the outer disk of M31 where one generally expects the long time scale events. Since concentration of variable stars towards longer period is higher as well as blending is more due to large seeing, microlensing candidates suffer from inhomogeneity in the light curve. We therefore explicitly check each light curve by eye and eliminated all those pixels which have periodic variability following Paulin-Henriksson et al. (2003). We further fit 5-parameters Paczyński fit on the R band data and non-linear least squares fit is estimated as

$$\chi^2 = \sum_{i=1}^n \frac{(\phi(t_i) - \phi_{fit}(t_i))^2}{\sigma^2(\phi(t_i))}$$

and determine the χ^2 per degree of freedom ($\bar{\chi}^2$). We reject those light curves which have $\bar{\chi}^2 > 4$. This left us with 7 pixels. To further check the achromaticity and symmetry in the selected pixels, we now use both R and I bands data together. We find that 5 of them are showing significant variation in I band while one of them is not showing synchronized variations in R and I bands as well as large value of half intensity duration hence needs further monitoring. This finally gives us one pixel which we have taken as a genuine microlensing candidate named as NMS-E1 where NMS is an acronym of the ‘Nainital

Table 1. Selection criteria to determine microlensing candidates.

Condition	pixels left
Masking bad pixels	80%
Bump detection	~ 19000
Clusterization of pixels	912
$(\chi^2/N)_{baseline} < 5$	670
$\bar{\chi}^2 < 4$	7
7-parameters fit	1

Microlensing Survey’. A summary of the selection criteria is given in Table 1.

4.2. Microlensing Candidate NMS-E1

We find microlensing candidate NMS-E1 at the pixel coordinate (880,1402) corresponding to $\alpha_{2000} = 00^h43^m33.3^s$, $\delta_{2000} = +41^\circ06'44''$ with an error of $\sim 1''$ in both α and δ . The candidate lies at an angular distance of $15'28''$ on the far side of disk from M31 center and its position in our frames are shown in Fig. 9. The source is unresolved at its minimum brightness in our observations as can be seen in the left side of the figure, however, it is clearly visible when it reached its maximum brightness which is shown in the right side of the figure. The R and I bands pixel light curves of NMS-E1 are shown in Fig. 10. A 7-parameters (i.e. full width at half maximum $t_{1/2}$, time of maximum amplification t_0 , impact parameter u_0 and baseline flux and stellar flux for both the bands) Paczyński fit to the pixel light curves gives a half duration time of $t_{1/2} \sim 59 \pm 2$ days with peak magnification time of $t_0 = 1908 \pm 1$ days.

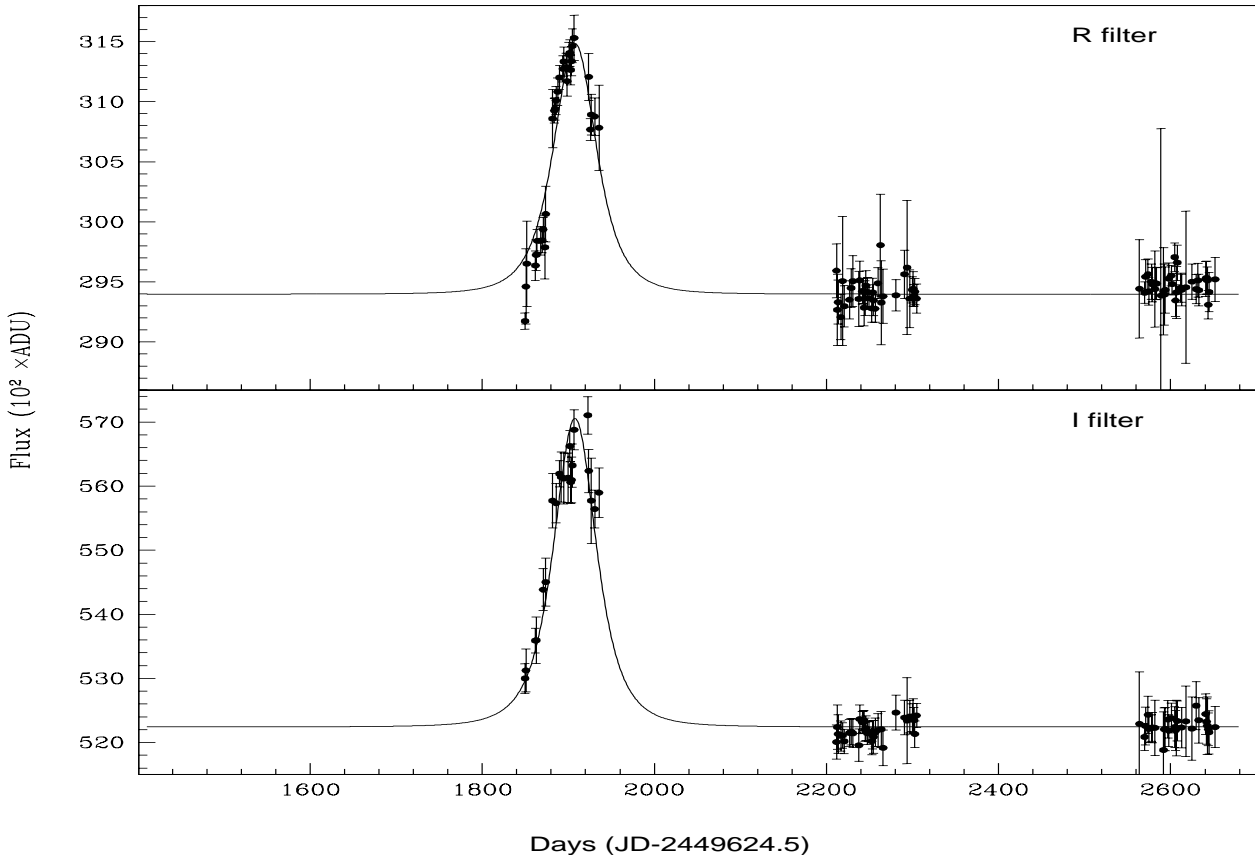


Fig. 10. The R and I band pixel light curves of NMS-E1 in upper and lower panels respectively. The continuous lines represent the results of 7-parameters Paczynski fit.

4.3. Shape analysis and achromaticity

A microlensing event possesses a characteristic Paczynski shape (Paczynski 1986) with a flat baseline and achromatic in nature. The event NMS-E1 does not strictly follows the symmetric shape as evident from Fig. 10. It is seen that the shape of light curve is broadened in I band in comparison of R band.

When we have seen pixels around (880,1402), we find a bright source at $\sim 2''.5$ to $\sim 5''.5$ away towards south-west direction which reach up to $R \sim 20.6$ magnitude having a mean $(R - I) \sim 1.3$. Its photometric analysis indicates that the source could be a red variable. We did not find any other bright star in our observations at the detection limit of $R \sim 21.5$ mag. When we analyse the light curve of same pixel in MDM data³ which is observed through 1.3 m telescope and a better seeing conditions, we see a bump in the light curve during 1998-1999 observing season along with a few overlapping points in the rising branch of microlensing candidate. We estimate the magnitude of the bump equivalent to

$$R(\Delta\phi) \sim 22.8; \quad I(\Delta\phi) \sim 20.7$$

³ The pixel coordinate corresponds to NMS-E1 in the MDM target field is (1227,451). The light curve for this pixel is kindly provided by the AGAPE collaboration.

This star seems very close to the candidate pixel and can not be resolved in our images. Though we cannot exactly estimate the magnitude of the star but its change in flux in the MDM light curve indicates that it is an extremely red variable. As each pixel of $\sim 2''.5 \times 2''.5$ area contains more than one thousand stars of M31, it is very likely that the nearby bright stars and red variables contaminate the pixel flux which not only deform the shape of light curve but may also change the achromatic nature of the event.

To test the achromatic nature and effect of blending on the candidate event NMS-E1, we have drawn a flux-flux diagram in Fig. 11. Though, the fit ($\chi^2/ndf = 1.6$) is linear for the upper portion of the light curve within our noise level but it shows a systematic increase of flux in $\Delta(\phi_I)$ around the fainter side of the microlensing regime which suggests that the light curve of NMS-E1, in general, is chromatic. However, keeping in mind the nearby red variable star contamination as we discussed earlier, it is not unusual. In the crowded regions like M31, it is quite difficult to separate out the noisy contribution from nearby variable sources. The effect of blending becomes more severe in I bands where the amplitude of variability is generally higher. The large and variable seeing as in our observations further worsens the contamination problem. Here we would like to point out that most of the pixel lensing candidates towards M31 are severely contaminated

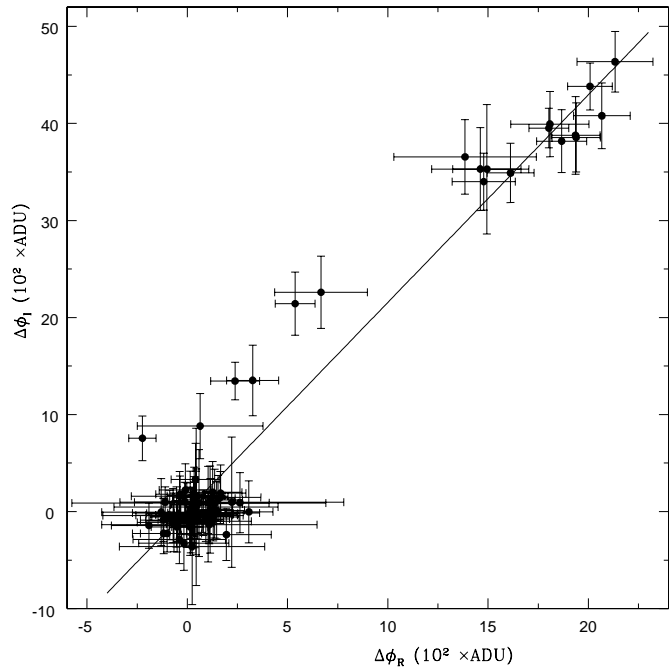


Fig. 11. A flux-flux variation of NMS-E1 where x- and y-axis show the increase of flux in R and I bands respectively. The points around $(0,0)$ indicate the base of the light curve. A continuous line indicates the best fit linear regression line.

by the nearby red variable stars which is also reflected in the various candidates reported by Calchi Novati et al. (2002, 2003), Paulin-Henriksson et al. (2002) and de Jong et al. (2003).

The physical parameters of NMS-E1 derived through pixel technique as well its photometric analysis are summarized in Table 2.

Table 2. Characteristics of the event NMS-E1.

α (J2000)	$00^h43^m33.3^s$
δ (J2000)	$+41^\circ06'44''$
distance from M31 center	$15'28''$
t_0	1908 ± 1
$t_{1/2}$	59 ± 2 days
R_{max}	20.1 mag
$(R - I)$	1.3 ± 0.2 mag
$\chi^2/d.f$	1.3

4.4. Physical interpretation of the event

We carry out photometry of NMS-E1 during its maximum brightness phase using DAOPHOT (Stetson 1987). The candidate reached its peak brightness in our observations on December 18, 1999 having magnitudes

$$R \sim 20.1; \quad I \sim 18.8; \quad (R - I) \sim 1.3$$

There can be an error of ~ 0.2 mag in the colour determination. Assuming a distance modulus of $(m - M)_0 = 24.49$ and extinction of $A_R = 0.63$, $A_I = 0.47$ towards our observed direction of M31 (Joshi et al. 2003), we estimate

$$M_R = -5.0; \quad M_I = -6.1; \quad (R - I)_0 = 1.1$$

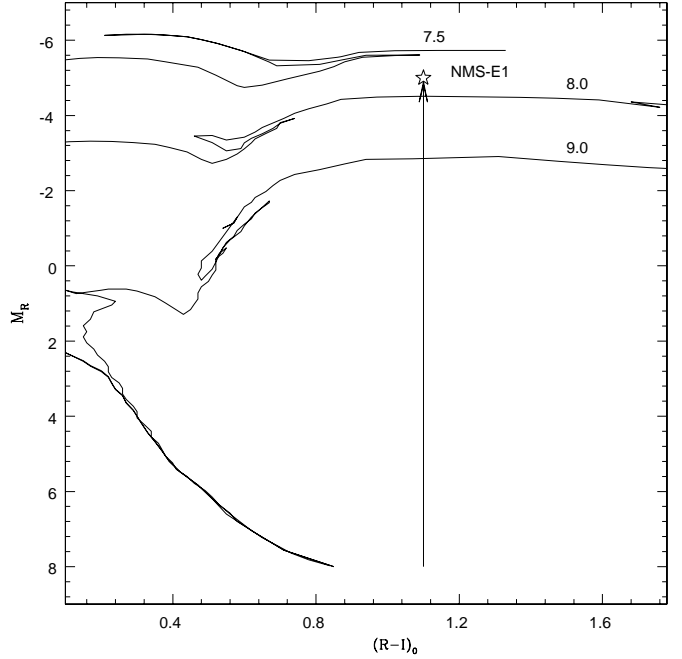


Fig. 12. The positions of NMS-E1 at its maximum brightness in the H-R diagram. The solar metallicity isochrones by Bertelli et al. (1994) for $\log A = 7.5, 8.0$ and 9.0 are also plotted. A vertical line is drawn to show the magnification direction.

The position of NMS-E1 in the H-R diagram is shown in Fig. 12. We can see that NMS-E1 is a very bright red star at its peak brightness which suggests that the source must lie either on the giant branch or it must be a M1-type main sequence (MS) star. If it is a MS star, its colour corresponds to an absolute magnitude of $M_R \sim 8$ mag (Cassisi et al. 1998) hence needs a very high magnification ($A_{max} > 10^5$) to reach a brightness of $M_R > -5$ mag. Since NMS-E1 is a long time scale event, the latter possibility is least likely. If it is a red giant star then we should be able to detect it in the Hubble Space Telescope (HST) images as HST is capable of detecting giant branch stars in M31. Unfortunately, there are no observations available for this region in the HST archive. Though the NMS-E1 is a long time scale event and red in colour, it is very unlikely that it is a Mira or any other long period variable as this event has been monitored for more than 800 days. This is one of the few pixel lensing events reported so far which is tracked for such a long duration that allowed us to rule out any possibility of it being a variable star.

Microlensing events which occur due to the objects in the halo of M31, have generally longer time scale than

the stars in the bulge or disk of M31 due to observer-lens-source geometry (Baltz et al. 2003). The high value of $t_{1/2}$ of NMS-E1 as well as its location in the far side of M31 disk indicate that the event might be due to halo lensing. The MEGA collaboration has also reported two long time scale microlensing candidates in the disk of M31 using differential technique i.e. ML-10 and ML-12 with the durations of $t_{1/2} \sim 47$ and 133 days respectively (de Jong et al. 2003). The candidate ML-10 lies in our observed field at an angular distance of $\sim 6'.6$ from position of NMS-E1 but shows a stable light curve in our data since we started observations when this event was almost merged with the background noise.

5. Discussion and Conclusions

The main difficulty in the pixel lensing search, in contrast to the conventional microlensing search, is that one cannot usually be able to measure the Einstein time t_E of the event from the observed pixel light curve which carry most of the physical information of the MACHO population. This is because the flux of normally unresolved star in the absence of the lensing is unknown. There is however one event PA-99-N1 reported by the POINT-AGAPE collaboration (Aurière et al. 2001, Paulin-Henriksson et al. 2003) where an unlensed star has been identified in HST archival images. We lack such kind of identification in the present study. Since we could not identify the source star, therefore, it is not possible for us to determine t_E and hence the mass of the lens. Nevertheless, by proper modeling of the stellar populations which either can be source stars or lens objects, we can estimate various parameters like timescale of microlensing events, their rate of occurrence and spatial distributions (de Jong et al. 2003). However, we need to detect a reasonable sample of genuine microlensing events along with prior knowledge of detection efficiency before making any conclusive estimates.

We have reported our first microlensing candidate detected through pixel technique on the far side of the galactic disk of M31. The peak brightness of the candidate $R_{max} \sim 20.1$ mag coupled with its colour $(R - I)_0 \sim 1.1$ and half intensity duration of $t_{1/2} \sim 59$ days lends support of it being a likely red giant source while main sequence star is highly improbable. The half intensity duration along with its location in M31 suggest that the event NMS-E1 might be due to halo lensing. Since we still have not estimated the detection efficiency, the likelihood of the event and results of Monte Carlo simulation will be discussed in a future publication. The variable stars of M31 have also been the subject of numerous studies e.g. star formation history, stellar population etc.; we are trying to compile a catalogue of pixel variables in our target field. If we do succeed, we would provide a detailed discussion in the future paper.

Here we presented the results of the pilot observational campaign carried out by us towards M31. We have been continuing our observations of the same field using a new 2-m Himalayan Chandra Telescope (HCT), Hanle, India

and we expect to find larger number of events which may enlighten us on the dark matter problem in the galactic halos of M31 and our own galaxy.

Acknowledgments We would like to thank B. Paczyński for his constructive comments which improved this paper. It is a great pleasure to thank Yannick Giraud-Héraud and Jean Kaplan for their kind support to initiate the project and get familiar with the pixel technique. DN is grateful to Japan Society for the Promotion of Science for an Invitation Fellowship. This study is a part of the project 2404-3 supported by Indo-French center for the Promotion of Advanced Research, New Delhi.

References

- Alard, C., & Lupton R. H., 1998, ApJ, 503, 325
- Alard, C., 2000, A&AS, 144, 363
- Alcock, C., Akerlof, C. W., Allsman, R. A., et al., 1993, Nature, 365, 621
- Alcock, C., Allsman, R. A., Alves, D. R., et al., 2000, ApJ, 542, 281
- Ansari, R., Aurière, M., Baillon, P., et al., 1997, A&A, 324, 843
- Aubourg, E., Bareyre, P., Brehin, S., et al., 1993, Nature, 365, 623
- Aurière, M., Baillon, P., Bouquet, A., et al., 2001, ApJ, 553, L137
- Bonanos, A. Z., Stanek, K. Z., Sasselov, D. D., et al., 2003, AJ, 126, 175
- Baillon, P., Bouquet, A., Kaplan, J., & Giraud-Héraud, Y., 1993, A&A, 277, 1
- Baltz, E. A., Gyuk, G., & Crotts, A. P. S., 2003, ApJ, 582, 30
- Bertelli, G., Bressan, A., Chiosi, C., Fagotto, F., & Nasi, E., 1994, A&AS, 106, 275
- Calchi Novati, S., Iovane, G., Marino, A. A., et al., 2002, A&A, 381, 848
- Calchi Novati, S., Jetzer, Ph., Scarpetta, G., et al., 2003, A&A, 405, 851
- Cassisi, S., Castellani, V., degl'Innocenti, S., & Weiss, A. 1998, A&AS, 129, 267
- Crotts, A. P. S., 1992, ApJ, 395, L25.
- Tomaney, A. B., & Crotts, A. P. S., 1996, AJ, 112, 2872
- de Jong, J. T. A., Kuijken, K. H., Crotts, A. P. S., et al., 2003, A&A, 417, 461
- Gould, A., 1996, ApJ, 470, 201
- Joshi, Y. C., Pandey, A. K., Narasimha, D., Sagar, R., & Giraud-Héraud, Y., 2003, A&A, 402, 113
- Joshi, Y. C., 2004, Ph.D Thesis, Kumaon University, Nainital, India
- Lasserre, T., Afonso, C., Albert, J. N., et al., 2000, A&A, 355, L39
- Paczyński, B., 1986, ApJ, 304, 1.
- Paulin-Henriksson, S., Baillon, P., Bouquet, A., et al., 2002, ApJ, 576, L121
- Paulin-Henriksson, S., Baillon, P., Bouquet, A., et al., 2003, A&A, 405, 15
- Press, W. H., & Rybici, G. B., 1989, ApJ, 338, 277
- Riffeser, A., Fliri, J., Bender, R., et al., 2003 ApJ, 599, L17.
- Stetson, B., 1987, PASP, 99, 191.
- Stanek, K. Z., & Garnavich, O. M., 1998, ApJ, 503, L131
- Taylor, S. F., 2004, PASP, 116, 1126
- Udalski, A., Szymanski, M., Kaluzny, J., et al., 1993, Acta Astron., 43, 289